OXFORD
SOT | Society of Toxicology
www.toxsci.oxfordjournals.org
Tox Spotlight article

TOXICOLOGICAL SCIENCES, 170(1), 2019, 144–156

doi: 10.1093/toxsci/kfz084
Advance Access Publication Date: March 28, 2019
Research Article

Copper-Induced Upregulation of MicroRNAs Directs the Suppression of Endothelial LRP1 in Alzheimer's Disease Model

Heng-Wei Hsu, Carlos J. Rodriguez-Ortiz, Siok Lam Lim, Joannee Zumkehr, Jason G. Kilian, Janielle Vidal, and Masashi Kitazawa[1]

Center for Occupational and Environmental Health (COEH), Department of Medicine, University of California, Irvine, California 92617-1830

[1]To whom correspondence should be addressed. Masashi Kitazawa, PhD, 100 Theory Dr., Suite 100, Irvine, CA 92617. E-mail: kitazawa@uci.edu.

ABSTRACT

Chronic exposure to copper and its dyshomeostasis have been linked to accelerated cognitive decline and potentially increasing risk for Alzheimer's disease (AD). We and others have previously demonstrated that exposure to copper through drinking water significantly increased parenchymal amyloid-beta (Aβ) plaques and decreased endothelial low-density lipoprotein receptor-related protein 1 (LRP1) in mouse models of AD. In this study, we determined the underlying mechanisms that microRNA critically mediated the copper-induced loss of endothelial LRP1. In human primary microvascular endothelial cells (MVECs), microRNA-200b-3p, -200c-3p, and -205-5p were significantly elevated within the 24-h exposure to copper and returned to baseline after 48-h postexposure, which corresponded with the temporal change of LRP1 expression in these cells. Transient expression of synthetic microRNA-200b-3p, -200c-3p, or -205-5p on MVECs significantly decreased endothelial LRP1, and cotreatment of synthetic antagomirs effectively prevented the loss of LRP1 during copper exposure, collectively supporting the key regulatory role of these microRNAs in copper-induced loss of LRP1. In mice, a significant reduction of LRP1 in cortical vasculature was evident following 9 months exposure to 1.3 ppm copper in drinking water, although the levels of cortical microRNA-205-5p, -200b-3p, and -200c-3p were only marginally elevated. This, however, correlated with increased vascular accumulation of Aβ and impairment of spatial memory, indicating that copper exposure has the pivotal role in the vascular damage and development of cognitive decline.

Key words: vasculature; amyloid-beta; mouse model; cognition; J20 mice.

Abnormal buildup of amyloid-beta (Aβ) species in the brain parenchyma is one of the early and pivotal pathological event preceding the development of neurofibrillary tangles, neuroinflammation, neurodegeneration, and cognitive decline in Alzheimer's disease (AD) (Bloom, 2014; Jack *et al.*, 2010). Although aging and genetic predispositions contribute greatly to the disease onset and are virtually perpetual within each individual, concordance for AD among homozygous twins is not 100% (Gatz *et al.*, 1997, 2006), strongly suggesting a putative involvement of modifiable environmental risk factors in the pathogenesis. In an effort of searching environmental risk factors, accumulating evidence indicates that excess exposure to copper (Cu) from the environment and Cu dyshomeostasis in the body, most notably by elevated levels of labile Cu, also known as unbound or free Cu in blood, are positively associated with poor cognitive performance, reduced CSF Aβ, and increased CSF tau as well as faster conversion from mild cognitive impairment (MCI) stage to clinically diagnosed AD stage (Squitti *et al.*, 2006, 2011, 2014; Talwar *et al.*, 2017; Ventriglia *et al.*, 2012; Vural *et al.*, 2010). Even among nondemented elderly population, excess Cu intake from dietary supplements or elevated levels of free Cu in blood is consistently associated with cortical thinning and impaired memory function (Morris *et al.*, 2006; Salustri *et al.*, 2010; Silbert *et al.*, 2018), suggesting a profound adverse effect of Cu

dyshomeostasis in the central nervous system and precursor to dementia. Although Cu is an essential transition metal serving as a catalytic cofactor for more than 20 redox enzymes (Itoh *et al.*, 2009), Cu from environment as inorganic cupric (Cu^{2+}) form may enter the blood stream and rapidly increase labile Cu levels to mediate potentially harmful events including the generation of reactive oxygen species in the local microenvironment (Brewer, 2015; Ceko *et al.*, 2014; Hill *et al.*, 1986; Hsu *et al.*, 2018; Medeiros, 2011; Prohaska, 2008). In fact, a very recent study using a mouse model of Down syndrome demonstrates that Cu is abnormally accumulated in cortex and hippocampus and exerts oxidative damage and cognitive decline (Ishihara *et al.*, 2019), although abnormal Cu accumulation in postmortem brains from AD or Down syndrome patients remains controversy (Miller *et al.*, 2006; Rembach *et al.*, 2013), and its neurotoxic mechanism of action is subject to further debates.

We and others have recently unveiled a novel toxic mechanism of Cu in AD by downregulating low-density lipoprotein receptor-related protein 1 (LRP1), one of the major receptors mediating the transcytosis of Aβ across the blood-brain barrier (Kang *et al.*, 2000; Silverberg *et al.*, 2010), in capillary endothelial cells (Kitazawa *et al.*, 2016; Singh *et al.*, 2013). The cell type-specific selective functional loss of LRP1 in the brain has been shown to cause aberrant parenchymal Aβ buildup in various mouse models of AD (Kanekiyo *et al.*, 2013; Liu *et al.*, 2017; Sagare *et al.*, 2013; Storck *et al.*, 2015; Zhao *et al.*, 2015). In humans, a significant loss of LRP1 in the brain is observed in advanced aging, MCI, and AD (Donahue *et al.*, 2006; Kang *et al.*, 2000; Silbert *et al.*, 2018; Sultana *et al.*, 2010), supporting its involvement in the pathogenesis. Earlier study showed that Cu-induced loss of endothelial LRP1 was mediated by proteasomal degradation (Singh *et al.*, 2013). Our recent findings implied an involvement of inflammation, particularly interleukin (IL)-1β, IL-6, and tumor necrosis factor-α, in Cu-induced impairment of phagocytosis and loss of LRP1 *in vitro*, predicting divergent toxic mechanisms of action of Cu.

In this study, we sought to elucidate the underlying mechanisms by which Cu downregulated LRP1 in endothelial cells, and we found microRNAs played a critical role in the loss of LRP1. Cu exposure resulted in significant upregulations of microRNA-205-5p, -200b-3p, and -200c-3p, and inhibition of these microRNAs during Cu exposure restored LRP1 levels *in vitro*. On the other hand, although these microRNAs were only marginally elevated in the mouse brain following chronic exposure to Cu, a significant reduction of vascular Lrp1 remained observed in these mice, and elevated levels of Aβ accumulation around vasculature were detected in J20 mice. These findings provide further mechanistic insights into our current understanding of Cu neurotoxicity and supported the view that alterations of microRNA dynamics and vascular damage in the brain may increase the risk for developing AD by interfering LRP1-mediated clearance of Aβ.

MATERIALS AND METHODS

Mice and chronic exposure to Cu containing drinking water. All animal procedures were performed in accordance with National Institutes of Health and University of California guidelines and Use Committee at the University of California, Irvine. Male and female wildtype (WT) C57BL/6J and J20 transgenic mice were used for chronic Cu exposure. Briefly, 1-month-old WT or J20 mice were divided into 2 groups (5 mice per sex per group), regular drinking water (control) group and 1.3 ppm $CuCl_2$-containing drinking water group. All mice received either regular drinking water or Cu containing water for 9 months. Water was replaced every 7 days, and each mouse was monitored regularly for glooming and behaviors. At the end of the exposure period, mice underwent a battery of behavior tests and brain tissue was collected following cardiac perfusion.

Cell culture and treatments. Human primary brain microvascular endothelial cells (MVECs) were purchased from Cell Systems (ACBRI 376, Kirkland, Washington) and maintained as previously described (Kitazawa *et al.*, 2016). As for cell transfection with mimics, cells were seeded at approximately 50% confluency in 6-well plates and, 24 h later, transfected with 8 nM hsa-miR-205-5p, 200b-3p, and 200c-3p mimics or human negative control 2 (MISSION microRNA Mimics, Sigma-Aldrich, St Louis, Missouri) using RNAiMAX according to manufacturer's instructions (No. 13778150, Thermo Fisher Scientific, Rockford, Illinois). As for transfection with miRNA inhibitors, cells were transfected with inhibitors using RNAiMAX for 24 h; then added Cu 0.5 μM to the same media for additional 24 h. After 48 h of total incubation time, cells were washed once with PBS, lysed with M-Per extraction buffer (200 μl, Thermo Fisher Scientific) complemented with proteases and phosphatases inhibitors (Sigma-Aldrich), incubated 5 min at RT with gently agitation and centrifuged at 10, 000 × g for 30 min at 4°C. Immunoblot or qRT-PCR was then performed, and all *in vitro* data were collected from at least 3 independent experiments in duplicates or triplicates.

Cytotoxicity assay. After the exposure, 250 μg/ml of 3-(4, 5-dimethylthiazol-2-yl)-2, 5- diphenyltetrazolium bromide was added. Cells were incubated in the humidified incubator for 3 h, allowing buildup of insoluble formazan. After the incubation, 100 μl of isopropanol-HCl solution (isopropanol: HCl = 100: 1) was added and mixed well to completely dissolve formazan. Absorbance at 570 nm was measured by the Spectromax plate reader (Molecular Devices) as described previously (Kitazawa *et al.*, 2016).

Assessment of spatial memory function. After 9 months of 1.3 ppm Cu-drinking water treatment, all mice were subjected to cognitive evaluation in the object location memory (OLM) test and Morris water maze (MWM). The apparatus used for the MWM task was a circular white tank (1.28-m diameter) and filled with water maintained at 21°C–23°C. The maze was located in a room containing several simple visual extra maze cues. Mice were trained to swim and find a 4-inch diameter circular clear Plexiglas platform submerged 1 cm beneath the surface of the water and invisible to the mice while swimming. On each training trial, mice were placed into the tank at 1 of 4 designated start points in a pseudorandom order. Mice were allowed to find and escape onto the platform. If mice failed to find the platform within 60 s, they were manually guided to the platform and allowed to remain there for 30 s. Each day, mice received 4 training sessions separated by intervals of 90 s under a warming lamp. The training period ended when the control group (water-treated WT) reached criterion (<25 s mean escape latency). The probe trial to examine retention memory was assessed 24 h after the last training trial. In the probe trials, the platform was removed from the pool, and mice were monitored by a ceiling-mounted camera directly above the pool during the 1-min period. All trials were recorded for subsequent analysis. The parameters measured during the probe trial included: (1) latency to cross the platform location and (2) number of platform location crosses.

OLM was performed as previously described (Vogel-Ciernia and Wood, 2014). Before training, mice were handled 1–2 min for 4 days and were habituated to the experimental apparatus 5 min to the OLM chamber for 6 consecutive days in the absence of objects. During the training trial, mice were placed in the experimental apparatus with 2 identical objects (OLM: 100-ml beakers, 2.5-cm diameter, and 4-cm height) and were allowed to explore these objects for 10 min. Twenty-four hours later, animals' retention was tested for 5 min. During the test, one copy of the familiar object was placed in the same location as during the training trial, and one copy of the familiar object was placed in the different location to the previous day within the box. All training and testing trials were video recorded and hand scored by individuals blind to animal treatments. Videos were analyzed for total exploration of objects in addition to the discrimination index (DI) [(time spent exploring object in new location – time spent exploring object in familiar location)/(total time exploring in both locations) × 100%]. Combinations and locations of objects were used in a balanced manner to reduce potential biases attributable to preference for particular locations.

Tissue preparation. After deep anesthesia with sodium pentobarbital, mice were perfused transcardially with 0.1 M phosphate-buffered saline (PBS), pH 7.4. Mice brains were dissected on ice, one hemisphere was pooled together and frozen with dry ice for biochemical analysis; the other hemisphere was collected for immunohistochemical staining. Protein extracts were prepared by homogenizing brain regions in T-Per extraction buffer (150 mg/ml, Thermo Fisher Scientific), complemented with proteases and phosphatases inhibitors (Sigma-Aldrich), and centrifuged at 10 000 × g for 30 min at 4°C. Protein concentration was determined from the supernatants using the Bradford assay following the manufacturer's protocol (Bio-Rad, Hercules, California).

Quantitative real time-PCR. Total RNA was purified from T-Per or M-Per lysates using Direct-zol RNA MiniPrep kit (Zymo Research, Irvine, California) following the manufacturer's instructions. Complementary DNA was produced from 500 ng RNA using microRNA synthesis kit (Applied Biological Materials, BC, Canada) for microRNAs or 1 μg RNA using iScript cDNA Synthesis kit (BioRad) for mRNAs following the manufacturer's instructions. For qPCR, cDNA (1/10 dilution) was amplified on a CFX Connect thermocycler (Biorad) using iTaq Universal SYBR green supermix (BioRad) on the following conditions. As for microRNAs: 95°C 10 min; 40× (95°C 15 s and 60°C 30 s); dissociation curve 65°C–95°C with 0.5°C increments every 5 s. mRNAs: 95°C 10 min; 35× (95°C 30 s, 60°C 1 min, and 72°C 1 min); dissociation curve 60°C–95°C with 0.5°C increments every 5 s. Data were normalized to RNA U6 small nuclear 1 (RNU6, for microRNAs) or glyceraldehyde 3-phosphate dehydrogenase (GAPDH, for mRNAs) levels. Primer sequences were selected using the Primer3 software. A complete list of the primer sequences used in this study is shown in Table 1.

Immunoblotting. Equal amounts of protein were separated on 4%–15% Bis-Tris gel and transferred to PVDF membranes. Membranes were blocked for 1 h in Odyssey blocking solution (Li-Cor, Lincoln, Nebraska). After blocking, membranes were incubated overnight with 1 or 2 of the following primary antibodies: LRP1 (1:25, Santa Cruz Biotechnology, California), GAPDH (1:5000, Santa Cruz Biotechnology), 6E10 (1:1000, Covance, Dedham, Massachusetts) CTFs (1:1000, Calbiochem, San Diego, California) in tris-buffered saline (TBS) Odyssey blocking solution + 0.2% tween-20 at 4°C. After washes with TBS + 0.1% tween-20, membranes were incubated for 1 h with the specific IRDye (Li-Cor) secondary antibodies in TBS + 5% Nonfat milk + 0.2% tween-20 + 0.01% SDS. Blots were scanned in an Odyssey infrared imager (Li-Cor). Image Studio software (Li-Cor) was used for protein quantification. Protein levels were normalized to GAPDH or tubulin.

Table 1. List of Primers Used in the Study

Primer	Sequence
microRNA-103a-3p	5′-AGCAGCATTGTACAGGGCTATGA-3′
microRNA-107	5′′-AGCAGCATTGTACAGGGCTATCA-3′
microRNA-200b-3p	5′-TAATACTGCCTGGTAATGATGA-3′
microRNA-200c-3p	5′-TAATACTGCCGGGTAATGATGGA-3′
microRNA-205-5p	5′-TCCTTCATTCCACCGGAGTCTG-3′
microRNA-429	5′-TAATACTGTCTGGTAAAACCGT-3′
RNU6	5′-AAATTCGTGAAGCGTTCCAT-3′
LRP1forward	5′-CAACGGCATCTCAGTGGACTAC-3′
LRP1 reverse	5′-TGTTGCTGGACAGAACCACCTC-3′
GAPDH forward	5′-GTCTCCTCTGACTTCAACAGCG-3′
GAPDH reverse	5′-ACCACCCTGTTGCTGTAGCCAA-3′

Meso scale discovery for Aβ detection. Meso scale discovery (MSD) V-PLEX (4G8) 96-well plate was purchased from Meso Scale Diagnostics, Maryland. Aβ40 and Aβ42 were detected following the manufacturer's instructions. Briefly, 150 μl blocker solution was added into each well and incubate at room temperature with shaker for 1 h. After washing the plate for 3 times, adding 25 μl detection antibody solution and 25 μl sample from mice cortex soluble fractions to each well and incubate at room temperature with shaker for 2 h. Wash the plate for another 3 times, then add 150 μl read buffer T to each well. Analyze the plate on an MSD instrument.

Quantitative Aβ enzyme-linked immunosorbent assay analysis. Soluble and insoluble Aβ1-40 and Aβ1-42 levels were measured by enzyme-linked immunosorbent assay (ELISA). Briefly, 96-well plates (Immulon 2HB, Fisher Scientific, Waltham, Massachusetts) were coated with 25 mg/ml of the mouse antiAβ monoclonal antibody (clone 20.1) in carbonate coating buffer pH 9.6 (Sigma-Aldrich) and incubated overnight at 4°C. The wells were washed and blocked with 3% bovine serum albumin (BSA) overnight at 4°C with shaking. After washing, serial dilutions of Aβ40 and Aβ42 were added to the wells and plates were sealed then incubated overnight at 4°C with shaking. After washing, horseradish peroxidase conjugated affinity antiAβ40 or antiAβ42 antibodies were added at 1:2000 and 1:1000 dilutions, respectively, and incubated overnight at 4°C with shaking. Wells were then washed and incubated with streptavidine horseradish peroxidase (1:4000 dilution) for 4 h at room temperature, washed then Ultra-TMB ELISA substrate (Pierce, Rockford, Illinois) was added for 5–10 min to develop the reaction. The reaction was stopped by adding 2 N H_3PO_4 and plates were analyzed on Synergy BioTek plate reader (BioTek Instruments, Winooski, Vermont) at 450 nm.

Immunohistochemical and immunofluorescence staining. Brain sections (40 μm) were mounted onto slides and washed with TBS twice, followed by blocking with 0.1% triton X-100 with 3% BSA and 5% goat serum in TBS for 1 h. Tissues were incubated with LRP1 primary antibody, FITC-cojugated lectin (1:500, Sigma-Aldrich), 4G8 and 6E10 (1:400, Covance Inc., Princeton, New

Jersey), Iba1 (1:1000, Wako, Richmond, Virginia), GFAP (1:1000, DAKO, Santa Clara, California) and 82E1 (1:1000, Immunobiological Laboratories, Gunma, Japan) overnight at 4°C. After washing with 0.1% triton X-100 in TBS twice, the sections were incubated with respective fluorescent secondary antibodies Alexa Fluor-488 and -555 (Molecular Probes) for 1 h at room temperature. The stained slides were photographed under an EVOS microscope attached with a digital camera. Five to six random fields of the cortex and hippocampus were selected to measure the ratio of LRP1/lectin-positive vessels and 5–6 mice were analyzed per group using ImageJ software.

Statistical analysis. All data were analyzed for statistical significance using 1-way analysis of variance followed by Bonferroni's multiple comparison post hoc test or unpaired Student's *t* test. We performed at least 3 separate experiments and all values were presented as mean ± SEM. A $p < .05$ is considered as significant.

RESULTS

Cu decreases LRP1 expression in human primary MVECs. We first determined the sustained downregulation of LRP1 following Cu exposure in human primary MVECs. Concentration of nonCp-bound free Cu in serum is estimated to be 0.2 μM (Singh *et al.*, 2013), and our previous study demonstrated that 0.5 μM Cu elicited exaggerated proinflammatory activation in response to Aβ42 without cytotoxicity in BV2 cells (Kitazawa *et al.*, 2016). Thus, we continued to use 0.5 μM Cu in MVECs and examined the temporal changes of LRP1 expression. MVECs were exposed to 0.5 μM Cu in the growth media for 24 h; then, allowed to recover for 0, 24, or 48 h in the normal growth media. The steady-state levels of LRP1 were significantly reduced by Cu exposure at 24 h, continued to be downregulated even after 24 h of recovery (24–24 h), and returned to the basal levels at 48 h (24–48 h) (Figure 1A). Similarly, LRP1 mRNA expression was found to be significantly reduced by Cu exposure and 24 h of recovery, while it was restored by 48 h of recovery (Figure 1B).

MicroRNA-205-5p, -200b-3p, and -200c-3p Were Predicted to Regulate LRP1 in MVECs Following Cu Exposure

In an effort of searching mechanisms of Cu-induced LRP1 downregulation, we found evidence showing microRNA-205 regulated LRP1 mRNA through silencing (Chan *et al.*, 2017; Song and Bu, 2009). We further predicted putative microRNAs that were conserved between mouse and human and interacted with 3'-untranslated region (3'UTR) of LRP1 mRNA using the TargetScan and miRanda (Betel *et al.*, 2008; Lewis *et al.*, 2005). Among a total of 7 candidate microRNAs that we screened (Table 1), microRNA-205-5p, -200b-3p, and -200c-3p were found to be significantly increased by 24 h exposure to Cu in MVECs (Figure 2A). These 3 microRNAs remained upregulated at 24 h of recovery and eventually returned to the basal levels at 48 h of recovery (Figs. 2B and 2C), correlating well with changes in LRP1 protein and mRNA described in Figure 1. Sequencing analysis confirms these 3 microRNAs have 8-base pair seed binding sequence in the 3'UTR of both human and mouse LRP1 mRNAs (Figure 3), which will then form a partially complementary binding to repress the translation of LRP1.

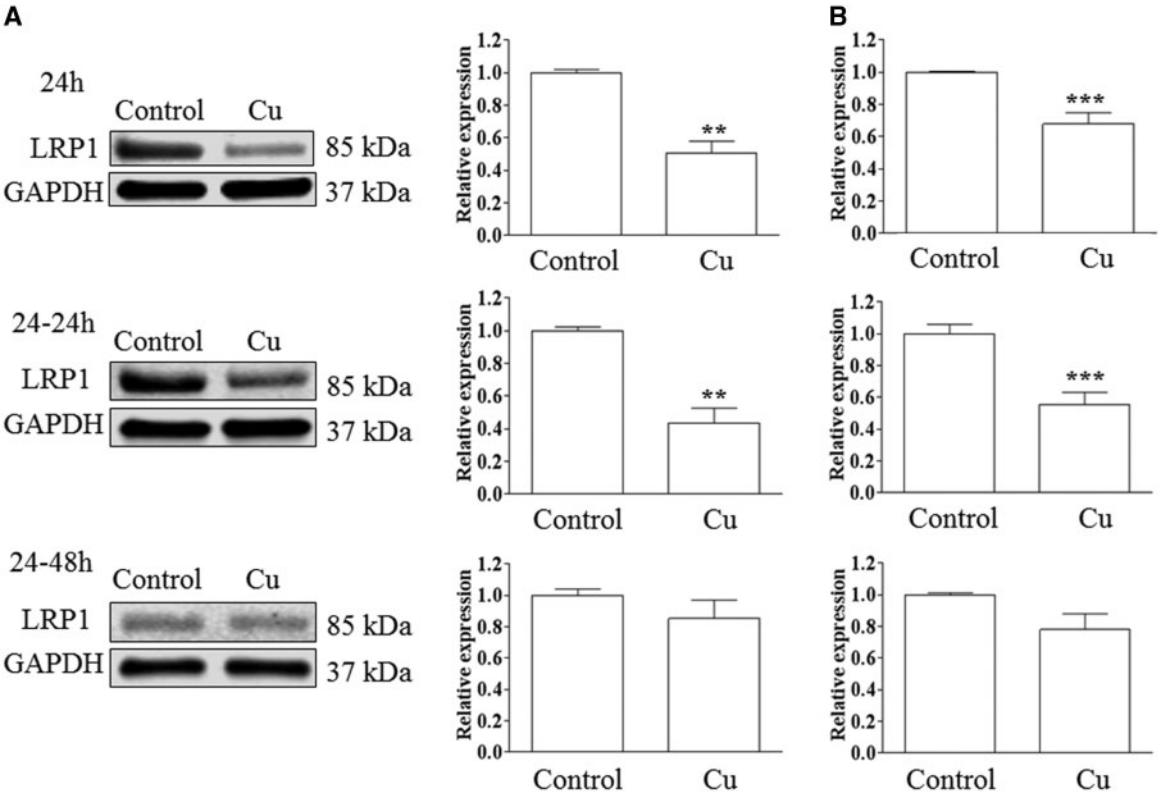

Figure 1. Cu reduced LRP1 levels in human primary MVECs. MVECs were exposed to 0.5 μM Cu for 24 h, then returned to normal growth media for additional 0 h (24 h), 24 h (24–24 h), or 48 h (24–48 h). A, The steady-state levels of LRP1 were significantly decreased at 24 h exposure and remained reduced even after 24 h rescue. Each graph represents mean ± SEM of 3 separate experiments in triplicates ($n = 9$ per group, $^{**}p < .01$ compared with the control group). B, Cu exposure significantly reduced LRP1 mRNA. Each graph represents mean ± SEM of 7 separate experiments in duplicates ($n = 14$ per group, $^{***}p < .001$ compared with the control group).

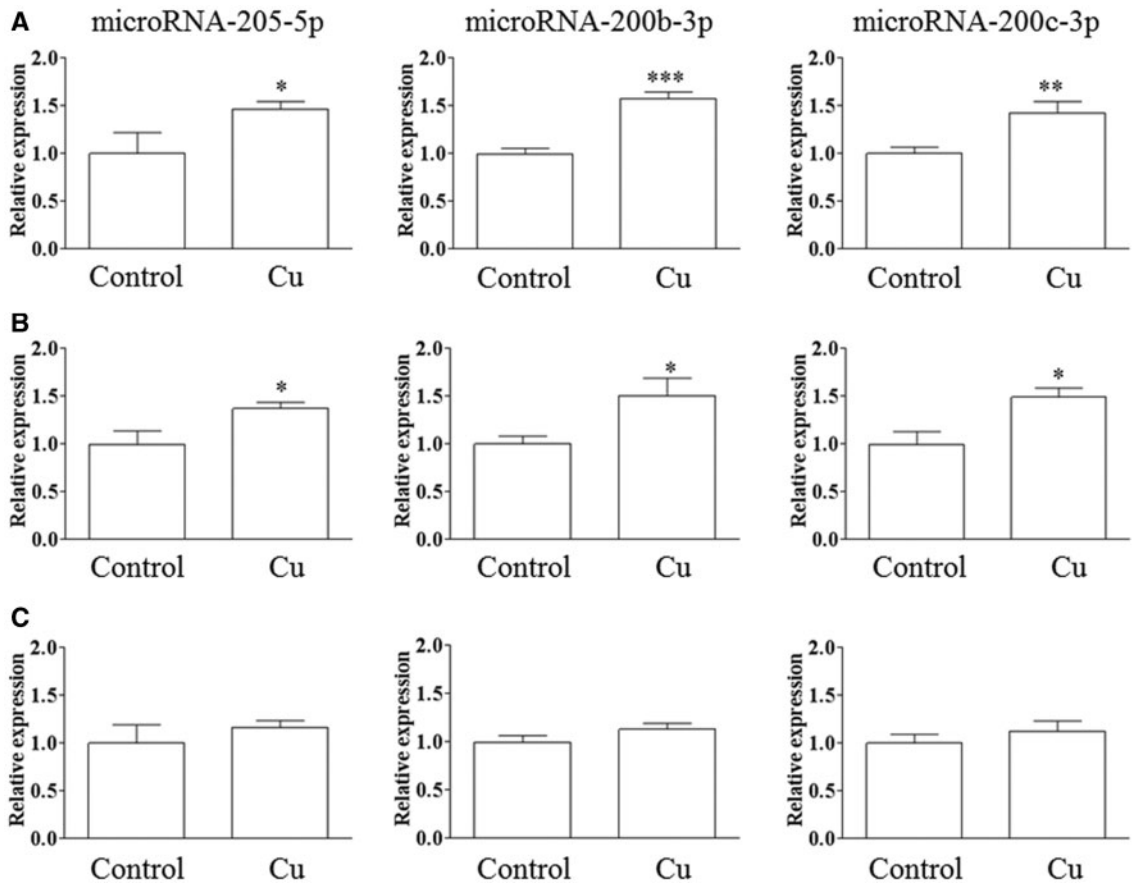

Figure 2. Mature microRNA-205-5p, -200b-3p, and -200c-3p were significantly elevated in MVECs exposed to Cu. MicroRNA-205-5p, -200b-3p, and -200c-3p transcripts were significantly elevated in MVECs following the exposure to 0.5 μM Cu for 24 h (A) and even after 24 h rescue (B), then returned to baseline after 48 h of rescue (C). Each graph represents mean ± SEM of 6 separate experiments in duplicates ($n = 12$ per group, $^{*}p < .05$, $^{**}p < .01$, or $^{***}p < .001$ compared with the control group).

Cu-Induced, microRNA-Mediated Downregulation of LRP1 in MVECs

To determine whether microRNA-205-5p, -200b-3p, and -200c-3p controlled LRP1 mRNA through posttranscriptional silencing in MVECs, we transiently overexpressed double-stranded RNA mimics of microRNA-205-5p, -200b-3p, or -200c-3p and analyzed the steady-state levels of LRP1 and LRP1 mRNA by qPCR. Forty-eight hours after the transfection with 8 nM of synthetic microRNA-205-5p, -200b-3p, or -200c-3p mimics in MVECs, we found a significant, around 50% reduction of LRP1 levels while a scramble sequence of microRNA mimics did not (Figure 4A), validating that these 3 microRNAs were capable of downregulating LRP1 independently. However, mimics treatment did not significantly affect LRP1 mRNA levels (Figure 4B). We next examined whether these 3 microRNAs were involved in Cu-induced downregulation of LRP1 in MVECs. Although application of individual synthetic miRNA antagomirs concomitantly with Cu exposure in MVECs did not effectively rescue the reduction of LRP1 (data not shown), combination of 3 synthetic miRNA antagomirs targeting microRNA-205-5p, -200b-3p, and -200c-3p effectively rescued the steady-state levels of LRP1 and LRP1 mRNA (Figs. 4C and 4D).

Chronic Cu Exposure Causes Loss of Brain LRP1 in Mice

In order to decipher a critical pathological role of microRNA in Cu-induced loss of LRP1 and development of AD phenotypes, we exposed 1-month-old WT C57BL/6J mice and J20 transgenic mice to 1.3 ppm Cu containing drinking water for 9 months and examined biochemical and histopathological features in the brain. Intriguingly, WT mice exposed to Cu significantly reduced the steady-state levels of LRP1 in cortex compared with control water-treated group by immunoblot while its reduction in J20 mice was not significant (Figure 5A). Levels of cortical microRNA-205-5p and -200b-3p, but not -200c-3p, were increased by approximately 1.5-fold relative to control group but failed to show statistical significance in WT mice (Figure 5B). In J20 mice, although we did not detect any significance between control and Cu groups, these 3 microRNAs were appeared to be elevated compared with WT control (Figure 5B). Changes of endothelial LRP1 in cortex were further examined by coimmunofluorescent staining. We found that a significant reduction of LRP1 staining on cortical cerebrovasculature in Cu-exposed WT and J20 mice while vascular staining by lectin remained fairly unchanged throughout the groups (Figure 5C), suggesting a cell type-specific reduction of LRP1 in the mouse brain by Cu exposure. Collectively, our results suggest neurotoxic effect of chronic Cu exposure that perturbed LRP1 in brain vasculature.

Changes in Neuroinflammation and Aβ Pathology in Cu-Exposed J20 Mice

The loss of endothelial LRP1 in cerebrovasculature has been reported to impair soluble Aβ40 clearance from the brain parenchyma in part because LRP1 possesses higher binding affinity to Aβ40 than Aβ42 (Bell *et al.*, 2007; Deane and Zlokovic, 2004; Storck *et al.*, 2015). We first examined whether the overall APP processing was altered by chronic Cu exposure in mice and

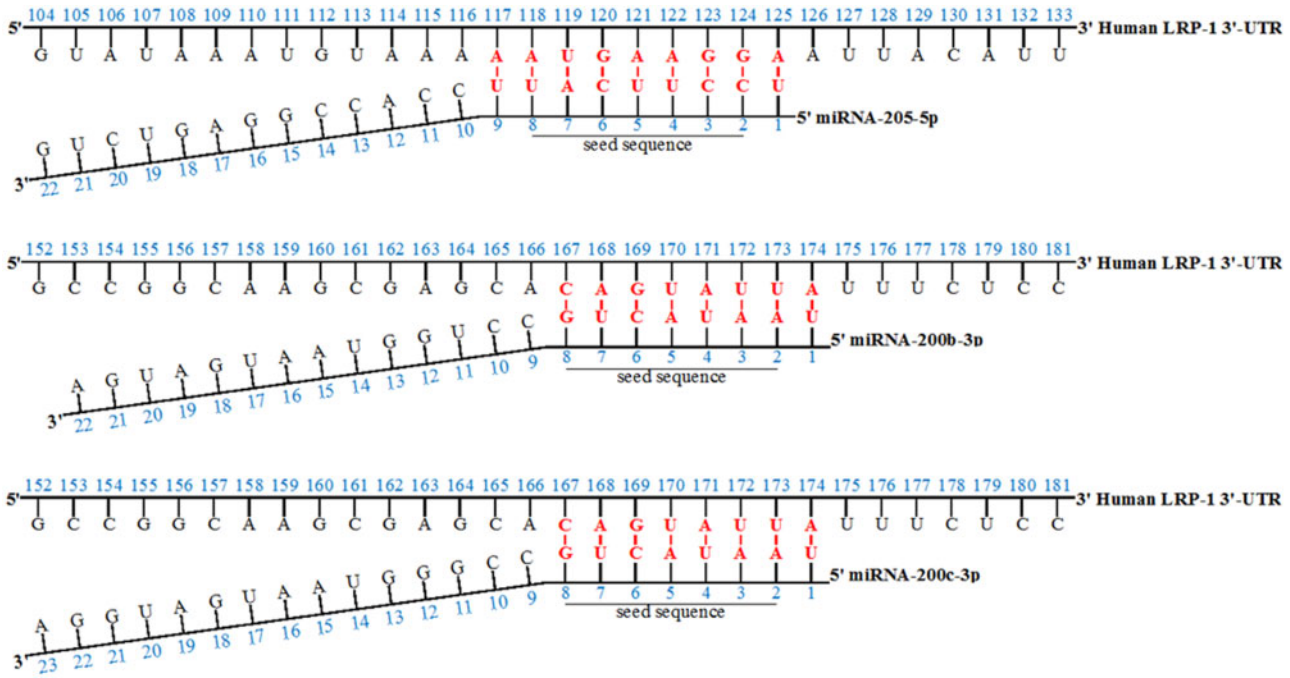

Figure 3. Schematic representation of the interaction between LRP1 3'UTR and the mature microRNA-205-5p, -200b-3p, and -200c-3p. Alignments between human LRP1 3'UTR and microRNA-205-5p, -200b-3p, and -200c-3p are illustrated. MicroRNA-205-5p forms a seed sequence with 117–125 nucleotides of LRP1 3'UTR, and microRNA-200b-3p and -200c-3p form a seed sequence with 167–174 nucleotides of LRP1 3'UTR. The same pairing is found in position 111–118 (for mouse microRNA-205-5p) and 156-163 (for mouse microRNA-200b-3p and -200c-3p) of the mouse LRP1 3'UTR. In addition, the mouse Lrp1 3'UTR has a second matching region for mouse microRNA-205-5p in the position 250–257 (not shown). Matching bases are shown in bold and the numbers indicate the position of the nucleotide within the 3'UTR or the mature microRNA. The seed sequence refers to nucleotides 2–8 of the microRNA. Predictions were generated using the TargetScan and miRanda.

found no significant change in the steady-state levels of full-length APP or its metabolites between control and Cu-exposed group (Supplementary Figure 1). Surprisingly, cortical deposition of Aβ plaques as well as soluble and insoluble Aβ40 and Aβ42 levels were not significantly different between control and Cu-exposed groups in WT or J20 mice (Supplementary Figure 2). Interestingly, however, neuroinflammation was significantly exacerbated in Cu-exposed mice as both Iba1+ microglia and GFAP+ astrocytes were increased in the cortical regions of Cu-exposed mice (Figure 6A). In J20 mice, we further investigated microglia and astrocyte activation around Aβ plaques and found that more microglia and astrocytes were residing in the vicinity of plaques in Cu-exposed J20 mice (Figure 6B). This may indicate increased inflammatory activation or dyshomeostasis triggered by chronic Cu exposure as we have previously reported *in vitro* (Kitazawa, *et al.*, 2016). Intriguingly, we also found a marked accumulation of Aβ peptides, detected by N-terminal specific Aβ antibody, in cerebrovasculature of the cortex of Cu-exposed J20 mice when compared with control J20 mice, especially where endothelial LRP1 was reduced (Figure 6C). Although it did not significantly contribute to the overall accumulation of soluble and insoluble Aβ species in the brain of 10 months old J20 mice, vascular accumulation of Aβ may be highlighted as one of the adverse effects elicited by Cu exposure in the brain.

Chronic Cu Exposure Exacerbates Spatial Memory in WT Mice

Extensive Aβ accumulation in cerebrovasculature can lead to cognitive decline and dementia. We tested spatial memory function by OLM and MWM in both WT and J20 mice after 9 months of Cu exposure through drinking water. Interestingly, Cu-exposed WT mice displayed significantly impaired DI in OLM compared with control group (Figure 7A). J20 mice, on the other hand, already exhibited impaired spatial memory at 10 months of age, and we did not find any further adverse performance in Cu-exposed group (Figure 7A). In MWM, while no difference was detected in mice with or without Cu exposure during acquisition (Figure 7B), retention memory was significantly impaired in WT mice exposed to Cu as measured by the latency to reach the platform location and the number of crosses (Figs. 7C and 7D). As expected, J20 mice exhibited impaired memory functions, and no difference was found by the exposure (Figs. 7C and 7D). Taken together, we presented that chronic Cu exposure reduced endothelial LRP1, possibly through upregulation of microRNA-200b-3p, -200c-3p, and -205-5p, and exacerbated vascular Aβ accumulation. Its direct impact to cognitive decline, however, needs further investigations.

DISCUSSION

Chronic exposure to environmentally relevant Cu in drinking water has previously been reported to significantly reduce LRP1 in the brain vasculature in mouse models of AD (Kitazawa *et al.*, 2016; Singh *et al.*, 2013). In this study, we further examined the underlying mechanism and found that microRNAs played a pivotal role in downregulating endothelial LRP1 expression in the presence of Cu. In human primary MVECs, Cu exposure significantly upregulated microRNA-205-5p, -200b-3p, -200c-3p from several more candidate microRNAs that were predicted to interact with the 3'UTR of LRP1 mRNA. During the recovery phase, the temporal pattern of the reduction of these microRNAs was inversely correlated with the restoration of LRP1 in the cell. Application of microRNA mimics and cotreatment of specific microRNA antagomirs with Cu further supported the direct involvement of these microRNAs on modulating endothelial LRP1.

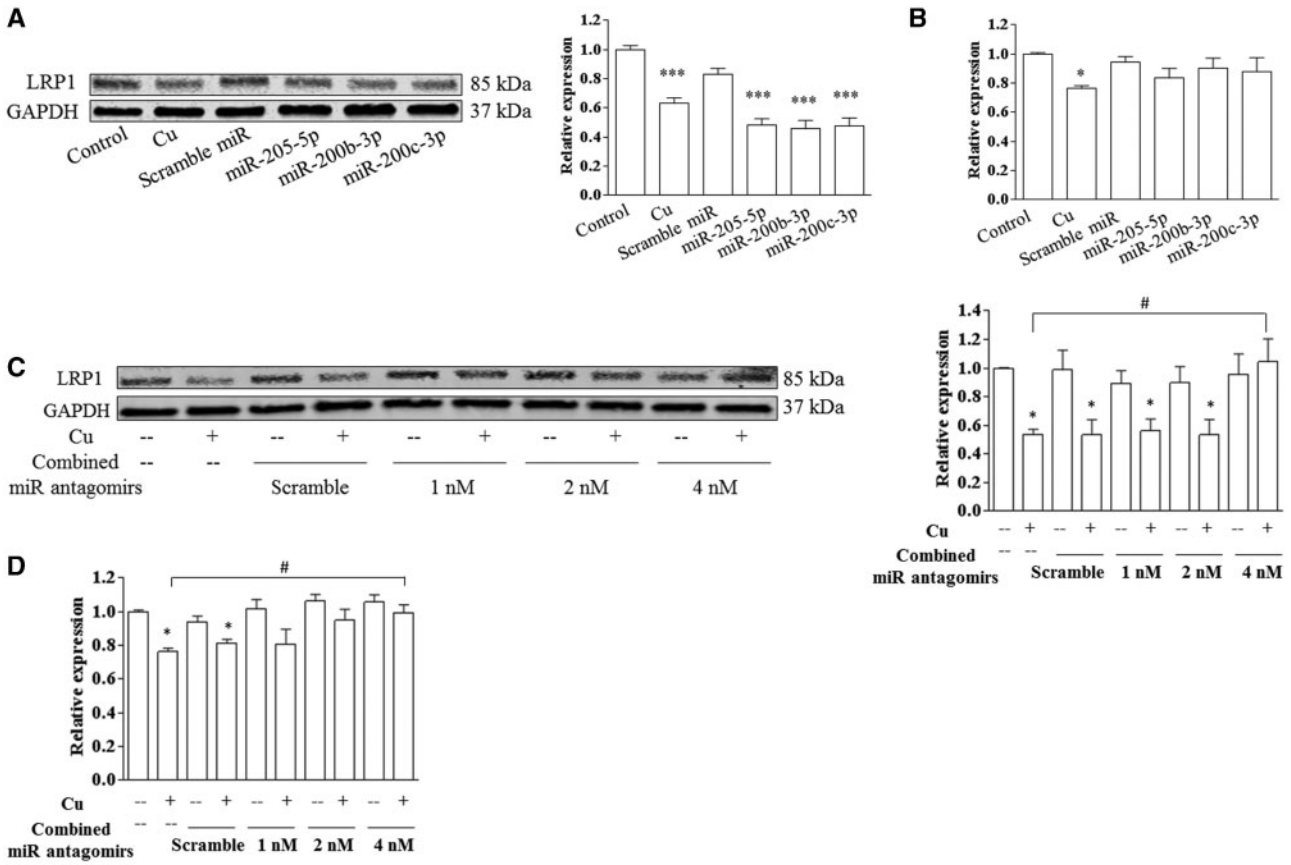

Figure 4. MicroRNA-205-5p, -200b-3p, and -200c-3p mediate Cu-induced LRP1 loss in MVECs. A, Transient transfection of synthetic miRNA-205-5p, -200b-3p, or -200c-3p mimics (8 nM), but not scramble microRNA control, significantly decreased the steady-state levels of LRP1, similar to those seen in Cu exposure, in MVECs. The graph represents mean ± SEM of 5 separate experiments in duplicates ($n = 10$ per group, $^{**}p < .01$, $^{***}p < .001$ compared with the control group). B, Synthetic microRNA mimics had no effect on the LRP1 transcript in MVECs. The graph represents mean ± SEM of 3 separate experiments in duplicates ($n = 6$ per group, $^{*}p < .05$ compared with the control group). C, The combined synthetic antagomirs (inhibitors) against microRNA-205-5p, -200b-3p, and -200c-3p (4 nM per antagomir) effectively restored the steady-state levels of LRP1 in the presence of Cu in MVECs. The graph represents mean ± SEM of 3 separate experiments in triplicates ($n = 9$ per group, $^{*}p < .05$ compared with corresponding control groups). D, Synthetic microRNA antagomirs restored LRP1 transcript in Cu -exposed MVECs. The graph represents mean ± SEM of 4 separate experiments in duplicates ($n = 8$ per group, $^{*}p < .05$ compared with the corresponding control group, and $\#p < .05$ compared between Cu-exposed group and Cu + 4 nM microRNA antagomirs group).

LRP1 has been shown to play critical roles in brain Aβ clearance, including in neurons (Kanekiyo *et al.*, 2013), astrocytes (Liu *et al.*, 2017), vascular mural cells (Kanekiyo *et al.*, 2012), and endothelial cells (Storck *et al.*, 2015). Age-related loss of endothelial LRP1 is well documented in humans as well as in early stages of AD, implicating that it is one of the initiating pathological changes leading to AD. In fact, growing bodies of evidence suggests that decreased turnover or clearance rate of Aβ from the brain, rather than overproduction of it, contributes to the accelerated buildup of Aβ and onset of AD (Lucey *et al.*, 2017; Mawuenyega *et al.*, 2010; Patterson *et al.*, 2015). Thus, Cu-induced development of AD pathology is in part due to an extensive loss of LRP1 and impairment of Aβ clearance mechanisms in the brain parenchyma. In order to incorporate the effect of chronic Cu exposure and normal aging process on potentially accelerated loss of LRP1 in cerebrovasculature in mouse models, we conducted 9-month exposure of 1.3 ppm Cu through drinking water and examined subsequent pathological changes in the brain. Intriguingly, we found a significant reduction of vascular endothelial LRP1 by genotype as well as by Cu exposure, suggesting a strong impact from the environment that could determine functional capacity of the vascular endothelial cells. These observed alterations may depend on the distribution of redox-active Cu in the body. If free Cu is elevated in blood as has been observed in humans (Salustri *et al.*, 2010; Silbert *et al.*, 2018; Squitti *et al.*, 2006, 2011, 2014; Talwar *et al.*, 2017; Ventriglia *et al.*, 2012; Vural *et al.*, 2010), vascular endothelial cells, which are in direct contact with blood, could be a primary target for Cu toxicity.

Although increased buildup of Aβ in the brain was predicted as a pathological consequence of the loss of endothelial LRP1 in mice (Storck *et al.*, 2015), parenchymal Aβ plaque burdens were largely unaffected in Cu-exposed J20 mice, and levels of brain microRNA-205-5p, -200b-3p, and -200c-3p were only marginally increased following chronic Cu-exposure. This apparent difference between our *in vitro* and *in vivo* findings may, in part, due to the following limitations and conditions. First, the *in vitro* data showed the changes of these miRNAs might be endothelial cell-specific responses. Thus, microRNA analysis using brain homogenates might mitigate any cell type-specific changes in mice. Second, these miRNAs that potentially perturb the ability to clear Aβ may play a key role in early and even prodromal stages of AD (Nagaraj *et al.*, 2017; Shinohara *et al.*, 2017). In fact, microRNA-205-5p in blood plasma has recently been identified as one of putative early biomarkers to predict AD (Kiko *et al.*, 2014). Last, multifaceted mechanisms could lead to loss of LRP1

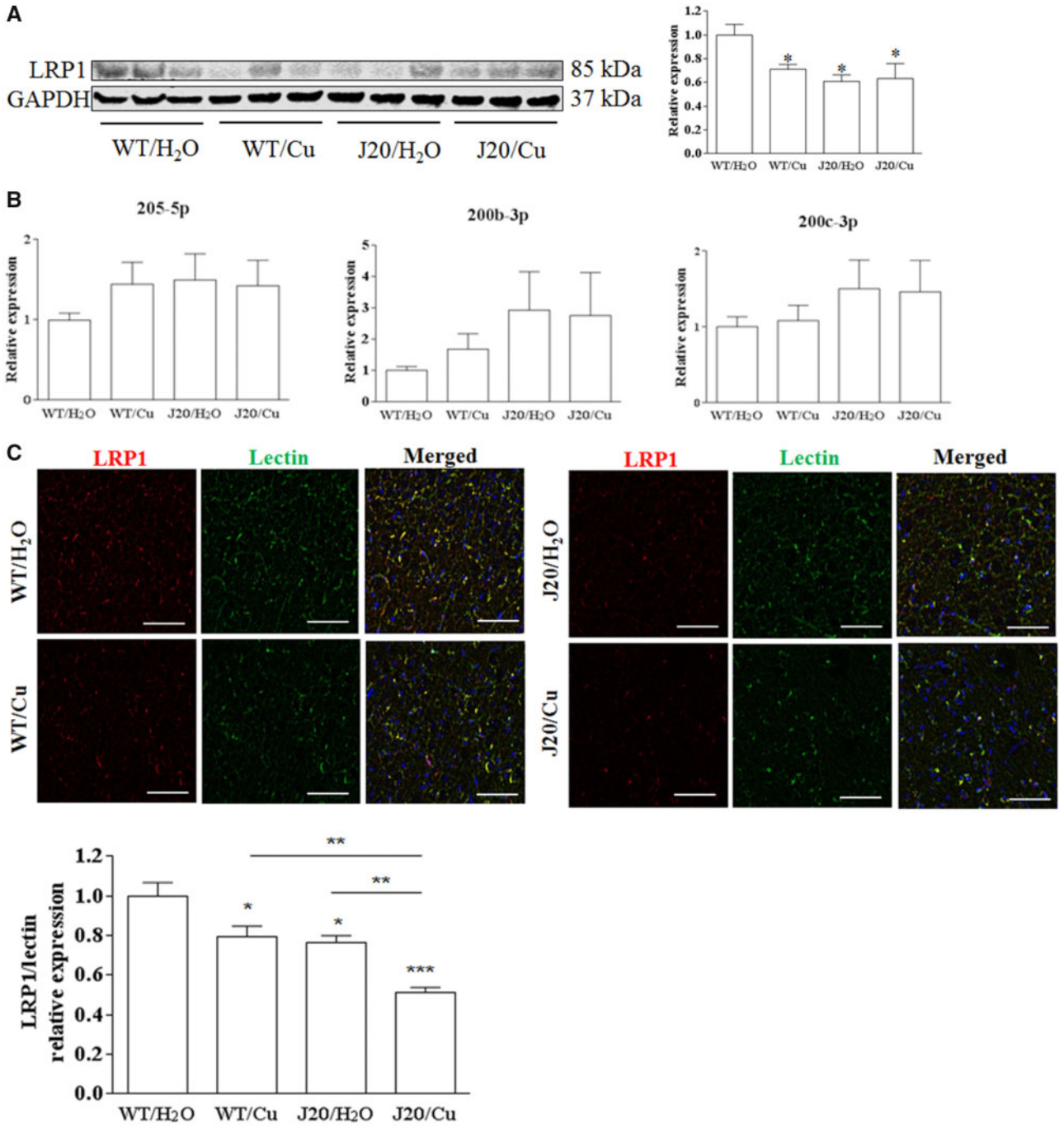

Figure 5. LRP1 decreased in the cortex following the chronic Cu exposure in mice. WT and J20 transgenic mice were exposed to 1.3 ppm Cu containing water for 9 months. A, The steady-state levels of LRP1 were significantly decreased in WT mice exposed to Cu (WT/Cu) compared with the control WT mice (WT/H_2O). Although J20 mice also showed a marked reduction of brain LRP1 (WT/H_2O vs J20/H_2O), no difference was detected between the Cu-exposed group (J20/Cu) and J20/H_2O. B, Total RNA extracted from cortex was used to analyze microRNA-205-5p, -200b-3p, and -200c-3p. No significant change in the levels of these microRNAs was detected in the cortex of WT mice and J20 mice regardless of exposure. Data for (A) and (B) were collected from $n = 9$–10 mice per group ($^*p < .05$ compared with WT control or WT/H_2O group). C, Vascular endothelial LRP1 in cortex was further detected by coimmunostaining of LRP1 (red) and lectin (endothelium, green) in all mice and found significantly reduced not only by genotype (WT vs J20) but also by Cu exposure within each genotype (H_2O vs Cu). Data were collected from $n = 5$ mice per group (scale bar: 200 μm, $^*p < .05$, $^{***}p < .001$ compared with the WT control or WT/H_2O group).

as a common outcome in highly heterogeneous brain tissues. Further studies will be essential in order to delineate the precise underlying mechanisms by which Cu downregulates LRP1 in cerebrovascular endothelial cells in mice. However, increased vascular Aβ accumulation, coupled with the loss of endothelial LRP1, is worth noting that there is a potential link between Cu exposure, vascular damage, and cognitive decline in the mouse model.

Recent mounting evidence strongly supports the pathological involvement of microRNA in AD and MCI (Lukiw *et al.*, 2012; Wu *et al.*, 2016). Change in microRNA profile in blood may serve as a biomarker to predict the disease progression

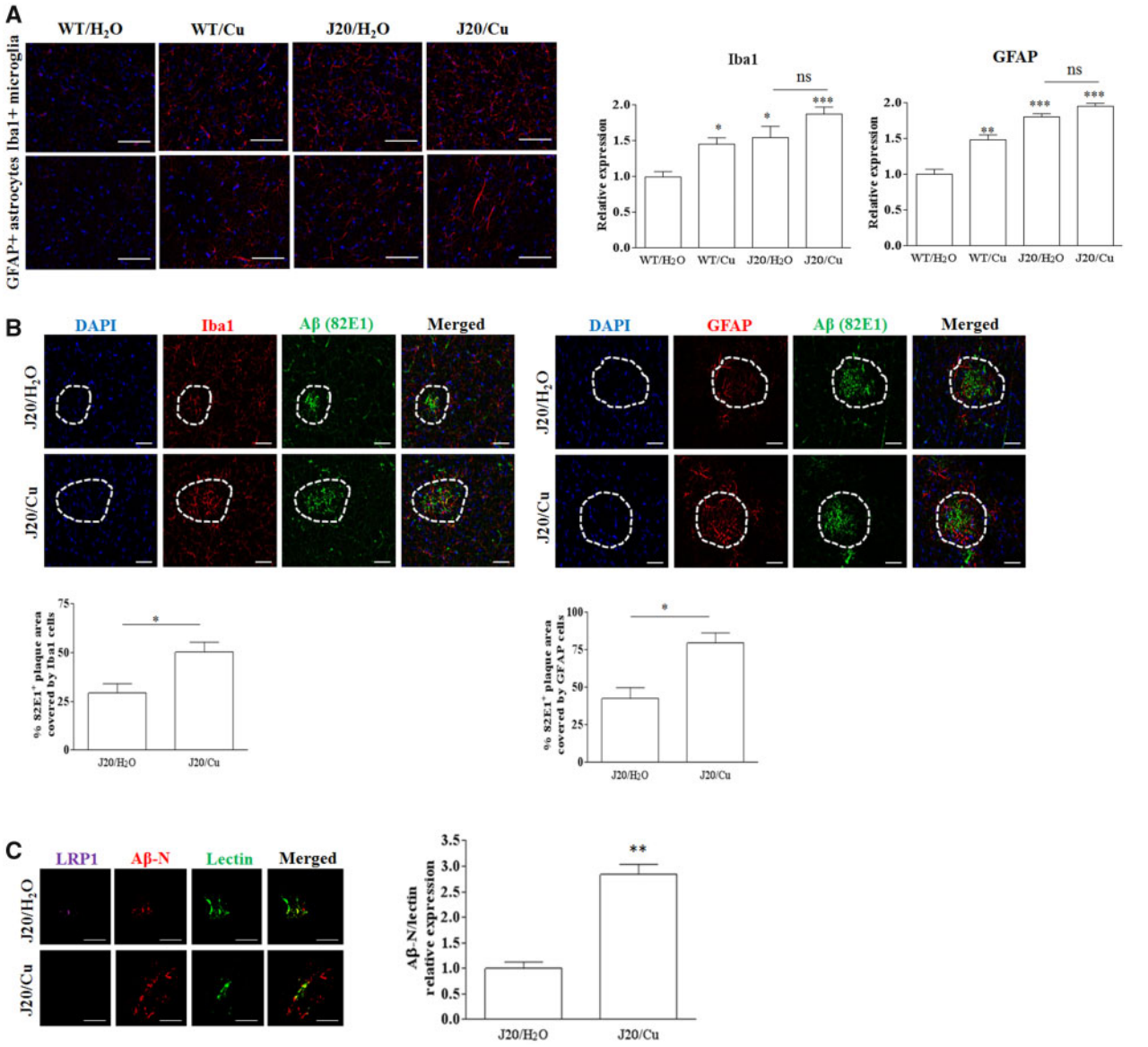

Figure 6. Cu exposure increased glial activation around Aβ plaques and vascular Aβ accumulation in mice cortices. A, Representative images of Iba1+ microglia (red) or GFAP+ astrocytes (red) staining with 4',6-diamidino-2-phenylindole (DAPI) nuclear staining (blue). Cu exposure enhanced glial activation particularly in WT mice (n = 4–5 mice per group, scale bar: 50 μm, $^{*}p < .05$, $^{**}p < .01$, $^{***}p < .001$ compared with WT/H_2O group). B, Quantitative analysis of percent 82E1+ plaque area covered by microglia (Iba1+) or astrocytes (GFAP+) revealed a significantly greater coverage within the 20 μm from the Aβ plaques in J20 mice exposed to Cu (J20/Cu) than in control J20 mice (J20/H_2O). Dotted lines outline regions at 20 μm from the edge of the plaques, where plaques and glial cells within the regions were quantified (n = 3 mice per group, scale bar: 20 μm, $^{*}p < .05$ compared with J20/H_2O group). C, Increased accumulation of Aβ around the vasculature was evident in J20 mice exposed to Cu. Coimmunostaining of LRP1 (purple), lectin (green), and Aβ-N (red) showed an increase of Aβ-N-positive plaques in the vicinity of capillary endothelium in J20/Cu group (n = 3–4 mice per group, scale bar: 50 μm, $^{**}p < .01$ compared with the J20 control or J20/H_2O group).

(Nagaraj *et al.*, 2017). Dysregulation of single microRNA could impact wide spectrum of the disease phenotypes including APP metabolism (Vilardo *et al.*, 2010), tau pathology (Banzhaf-Strathmann *et al.*, 2014; Cogswell *et al.*, 2008; Hébert *et al.*, 2010), lipid metabolism (Kim *et al.*, 2015), inflammation (Li *et al.*, 2011; Zhao *et al.*, 2014), and synaptic plasticity (Lee *et al.*, 2012; Rodriguez-Ortiz *et al.*, 2014). Although these miRNAs have been reported to be altered in AD, the trend of the changes is still controversial. Some group has reported that miR-200b was down-regulated (Liu *et al.*, 2014), while others have observed the opposite result (Guedes *et al.*, 2015). Liu found that the level of miR-200b was decreased in the hippocampi of 3-month APP/PS1 transgenic mice, suggesting that the change of miR-200b is earlier than the formation of amyloid plaques (Liu *et al.*, 2014). On the other hand, Guedes showed that miR-200b upregulated in blood-derived monocytes from AD patients, particularly, miR-200b could bind to the 3'UTR of beta-1, 4-mannosyl-glycoprotein 4-beta-N-acetylglucosaminyltransferase (MGAT3) (Guedes *et al.*, 2015). Downregulation of MGAT3 may relate to defective Aβ phagocytosis (Fiala *et al.*, 2007), suggesting a link between miR-200b upregulation, MGAT3 downregulation, impairment in Aβ phagocytosis and decreased Aβ clearance in AD.

In our study, we observed that miR-200b-3p and miR-200c-3p had similar effects on LRP1 downregulation. Both miR-200b and miR-200c are predicted to bind a highly overlapping range of targets and may therefore represent similar sequences, only

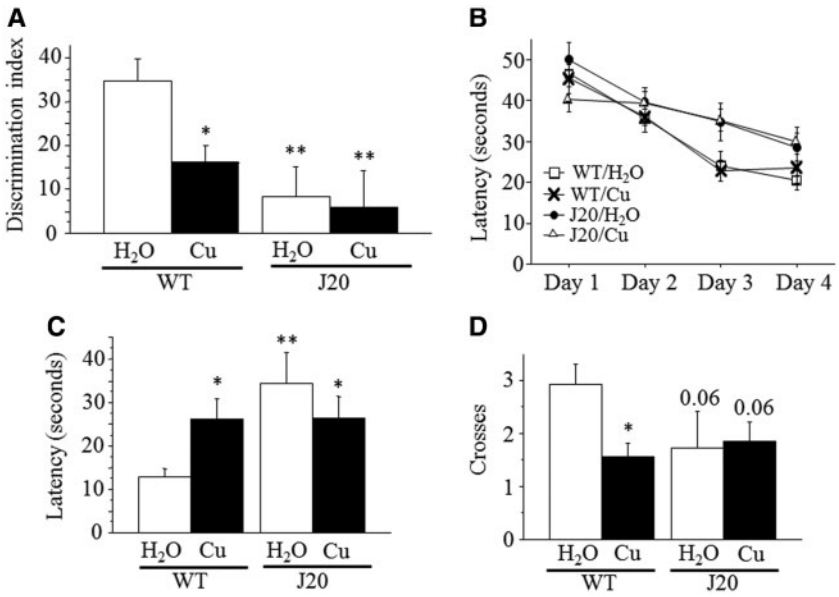

Figure 7. Chronic Cu exposure through drinking water exacerbates spatial memory. WT C57BL/6J mice and J20 mice were tested for spatial memory function after 9 months of Cu exposure. A, OLM test revealed a significant impairment of spatial memory function in WT mice exposed to Cu containing drinking water. B, In the acquisition of MWM test, there was a genotype difference but not by treatment group. On the other hand, during retention memory probe trial, Cu-exposed WT mice significantly exacerbated the latency to cross the platform location (C) and the number of crosses on the platform location (D), while no difference was detected in J20 mice ($n = 11$–16 per group, $^{*}p < .05$, $^{**}p < .01$ compared with WT control water-treated group).

a few nucleotides difference, they exert similar function. However, there are some discrepancies about their cellular role in previous literatures. Wu reported that miR-200c plays a protective role for neuronal survival and differentiation in response to Aβ-induced endoplasmic reticulum-stress. When Aβ was accumulated to a threshold, the apoptosis program started and miR-200c would decrease. The increase of miR-200c was detected from the sera of early stage of APP/PS mice and AD patients; in late stage of the disease, miR-200c level decreased (Wu *et al.*, 2016). As for other neurodegenerative diseases, miR-200b greatly decreased as well as dendritic spine densities reduction in prion disease mice (Boese *et al.*, 2016). In another study, increased miR-200c significantly upregulated at the presymptomatic stage in a huntingtin disease mouse model. MiR-200c could control genes involved in mutant HTT-induced neuronal dysfunction, including abnormal synaptic transmission, and disturbed neurogenesis (Jin *et al.*, 2012). In Parkinson's disease patients, miR-205 expression decreased and could be a potential biomarker for movement disorder (Cho *et al.*, 2013; Marques *et al.*, 2017). Meanwhile, miR-205 would decrease and upregulate TGF-β signaling in glioma cell line U87 and glioma patients' sera (Duan and Chen, 2016; Yue *et al.*, 2016). On the other hand, increased miR-205 expression induced by inflammation further downregulated LRP1 has been reported in atherosclerosis and abdominal aortic aneurysm (Chan *et al.*, 2017; Kim *et al.*, 2014; Son *et al.*, 2017). As noted in these reports, discrepancies may be related to factors that include accuracy of the diagnosis, samples acquisition and processing, tissue region analyzed, methodologies used in the analysis, intrinsic human individuality and different stages of the disease. Nevertheless, more studies needed to elucidate whether miRNA could be a reliable biomarker for AD in the future.

In conclusion, our study supports the putative role of microRNA-205-5p, miR-200b-3p, and miR-200c-3p involved in downregulating endothelial LRP1 expression after chronic Cu exposure. Although the pathogenic contribution of environmental risk factors, like Cu exposure, to AD remains controversial, recent evidence supports Cu dyshomeostasis leads to accelerated cognitive decline and possibly neuronal death (Silbert *et al.*, 2018; Yu *et al.*, 2018), which eventually promotes the onset of AD. Our study may unveil one underlying mechanism by which Cu exacerbates AD pathology through microRNA-mediated loss of LRP1.

SUPPLEMENTARY DATA

Supplementary data are available at *Toxicological Sciences* online.

FUNDING

This study was supported by National Institutes of Health/National Institute of Environmental Health Sciences (NIEHS) (R01 ES024331 to M.K.), Alzheimer's Association (AARF-16-442963 to H.W.H), and Alzheimer's Association (MNIRGD-15-363229 to C.J.R).

DECLARATION OF CONFLICTING INTERESTS

The authors declared no potential conflicts of interest with respect to the research, authorship, and/or publication of this article.

REFERENCES

Ban zhaf-Strathmann, J., Benito, E., May, S., Arzberger, T., Tahirovic, S., Kretzschmar, H., Fischer, A., and Edbauer, D. (2014). MicroRNA-125b induces tau hyperphosphorylation and cognitive deficits in Alzheimer's disease. *EMBO J.* **33**, 1667–1680.

Bell, R. D., Sagare, A. P., Friedman, A. E., Bedi, G. S., Holtzman, D. M., Deane, R., and Zlokovic, B. V. (2007). Transport pathways

for clearance of human Alzheimer's amyloid beta-peptide and apolipoproteins E and J in the mouse central nervous system. *J. Cereb. Blood Flow Metab.* **27**, 909–918.

Betel, D., Wilson, M., Gabow, A., Marks, D. S., and Sander, C. (2008). The microRNA.org resource: Targets and expression. *Nucleic Acids Res.* **36**, D149–D153.

Bloom, G. S. (2014). Amyloid-β and tau: The trigger and bullet in Alzheimer disease pathogenesis. *JAMA Neurol.* **71**, 505–508.

Boese, A. S., Saba, R., Campbell, K., Majer, A., Medina, S., Burton, L., Booth, T. F., Chong, P., Westmacott, G., Dutta, S. M., *et al.* (2016). MicroRNA abundance is altered in synaptoneurosomes during prion disease. *Mol. Cell Neurosci.* **71**, 13–24.

Brewer, G. (2015). Copper-2 ingestion, plus increased meat eating leading to increased copper absorption, are major factors behind the current epidemic of Alzheimer's disease. *Nutrients* **7**, 5513.

Ceko, M. J., Aitken, J., and Harris, H. H. (2014). Speciation of copper in a range of food types by X-ray absorption spectroscopy. *Food Chem.* **164**, 50–54.

Chan, C. Y. T., Chan, Y. C., Cheuk, B. L. Y., and Cheng, S. W. K. (2017). Clearance of matrix metalloproteinase-9 is dependent on low-density lipoprotein receptor-related protein-1 expression downregulated by microRNA-205 in human abdominal aortic aneurysm. *J. Vasc. Surg.* **65**, 509–520.

Cho, H. J., Liu, G., Jin, S. M., Parisiadou, L., Xie, C., Yu, J., Sun, L., Ma, B., Ding, J., Vancraenenbroeck, R., *et al.* (2013). MicroRNA-205 regulates the expression of Parkinson's disease-related leucine-rich repeat kinase 2 protein. *Hum. Mol. Genet.* **22**, 608–620.

Cogswell, J. P., Ward, J., Taylor, I. A., Waters, M., Shi, Y., Cannon, B., Kelnar, K., Kemppainen, J., Brown, D., Chen, C., *et al.* (2008). Identification of miRNA changes in Alzheimer's disease brain and CSF yields putative biomarkers and insights into disease pathways. *J. Alzheimers Dis.* **14**, 27–41.

Deane, R., Wu, Z., and Zlokovic, B. V. (2004). RAGE (yin) versus LRP (yang) balance regulates Alzheimer amyloid beta-peptide clearance through transport across the blood-brain barrier. *Stroke* **35**, 2628–2631.

Donahue, J. E., Flaherty, S. L., Johanson, C. E., Duncan, J. A., Silverberg, G. D., Miller, M. C., Tavares, R., Yang, W., Wu, Q., Sabo, E., *et al.* (2006). RAGE, LRP-1, and amyloid-beta protein in Alzheimer's disease. *Acta Neuropathol.* **112**, 405–415.

Duan, Y., and Chen, Q. (2016). TGF-β1 regulating miR-205/miR-195 expression affects the TGF-β signal pathway by respectively targeting SMAD2/SMAD7. *Oncol. Rep.* **36**, 1837–1844.

Fiala, M., Liu, P. T., Espinosa-Jeffrey, A., Rosenthal, M. J., Bernard, G., Ringman, J. M., Sayre, J., Zhang, L., Zaghi, J., Dejbakhsh, S., *et al.* (2007). Innate immunity and transcription of MGAT-III and Toll-like receptors in Alzheimer's disease patients are improved by bisdemethoxycurcumin. *Proc. Natl. Acad. Sci. U.S.A.* **104**, 12849–12854.

Gatz, M., Pedersen, N., Berg, S., Johansson, B., Johansson, K., Mortimer, J. A., Posner, S. F., Viitanen, M., Winblad, B., and Ahlbom, A. (1997). Heritability for Alzheimer's disease: The study of dementia in Swedish twins. *J. Gerontol. A Biol. Sci. Med. Sci.* **52**, M117–M125.

Gatz, M., Reynolds, C. A., Fratiglioni, L., Johansson, B., Mortimer, J. A., Berg, S., Fiske, A., and Pedersen, N. L. (2006). Role of genes and environments for explaining Alzheimer disease. *Arch. Gen. Psychiatry* **63**, 168–174.

Guedes, J. R., Santana, I., Cunha, C., Duro, D., Almeida, M. R., Cardoso, A. M., de Lima, M. C. P., and Cardoso, A. L. (2015). MicroRNA deregulation and chemotaxis and phagocytosis impairment in Alzheimer's disease. *Alzheimers Dement. (Amst.)* **3**, 7–17.

Hébert, S. S., Papadopoulou, A. S., Smith, P., Galas, M.-C., Planel, E., Silahtaroglu, A. N., Sergeant, N., Buée, L., and De Strooper, B. (2010). Genetic ablation of Dicer in adult forebrain neurons results in abnormal tau hyperphosphorylation and neurodegeneration. *Hum. Mol. Genet.* **19**, 3959–3969.

Hill, G. M., Brewer, G. J., Juni, J. E., Prasad, A. S., and Dick, R. D. (1986). Treatment of Wilson's disease with zinc. II. Validation of oral 64copper with copper balance. *Am. J. Med. Sci.* **292**, 344–349.

Hsu, H.-W., Bondy, S. C., and Kitazawa, M. (2018). Environmental and dietary exposure to copper and its cellular mechanisms linking to Alzheimer's disease. *Toxicol. Sci.* **163**, 338–345.

Ishihara, K., Kawashita, E., Shimizu, R., Nagasawa, K., Yasui, H., Sago, H., Yamakawa, K., and Akiba, S. (2019). Copper accumulation in the brain causes the elevation of oxidative stress and less anxious behavior in Ts1Cje mice, a model of Down syndrome. *Free Radic. Biol. Med.* **134**, 248–259.

Itoh, S., Ozumi, K., Kim, H. W., Nakagawa, O., McKinney, R. D., Folz, R. J., Zelko, I. N., Ushio-Fukai, M., and Fukai, T. (2009). Novel mechanism for regulation of extracellular SOD transcription and activity by copper: Role of antioxidant-1. *Free Radic. Biol. Med.* **46**, 95–104.

Jack, C. R., Jr, Knopman, D. S., Jagust, W. J., Shaw, L. M., Aisen, P. S., Weiner, M. W., Petersen, R. C., and Trojanowski, J. Q. (2010). Hypothetical model of dynamic biomarkers of the Alzheimer's pathological cascade. *Lancet Neurol.* **9**, 119–128.

Jin, J., Cheng, Y., Zhang, Y., Wood, W., Peng, Q., Hutchison, E., Mattson, M. P., Becker, K. G., and Duan, W. (2012). Interrogation of brain miRNA and mRNA expression profiles reveals a molecular regulatory network that is perturbed by mutant huntingtin. *J. Neurochem.* **123**, 477–490.

Kanekiyo, T., Cirrito, J. R., Liu, C.-C., Shinohara, M., Li, J., Schuler, D. R., Shinohara, M., Holtzman, D. M., and Bu, G. (2013). Neuronal clearance of amyloid-β by endocytic receptor LRP1. *J. Neurosci.* **33**, 19276–19283.

Kanekiyo, T., Liu, C. C., Shinohara, M., Li, J., and Bu, G. (2012). LRP1 in brain vascular smooth muscle cells mediates local clearance of Alzheimer's amyloid-β. *J. Neurosci.* **32**, 16458–16465.

Kang, D. E., Pietrzik, C. U., Baum, L., Chevallier, N., Merriam, D. E., Kounnas, M. Z., Wagner, S. L., Troncoso, J. C., Kawas, C. H., Katzman, R., *et al.* (2000). Modulation of amyloid β-protein clearance and Alzheimer's disease susceptibility by the LDL receptor–related protein pathway. *J. Clin. Invest.* **106**, 1159–1166.

Kiko, T., Nakagawa, K., Tsuduki, T., Furukawa, K., Arai, H., and Miyazawa, T. (2014). MicroRNAs in plasma and cerebrospinal fluid as potential markers for Alzheimer's disease. *J. Alzheimers Dis.* **39**, 253–259.

Kim, C. W., Kumar, S., Son, D. J., Jang, I.-H., Griendling, K. K., and Jo, H. (2014). Prevention of abdominal aortic aneurysm by anti-microRNA-712 or anti-microRNA-205 in angiotensin II-infused mice. *Arterioscler., Thromb. Vasc. Biol.* **34**, 1412–1421.

Kim, J., Yoon, H., Horie, T., Burchett, J. M., Restivo, J. L., Rotllan, N., Ramírez, C. M., Verghese, P. B., Ihara, M., Hoe, H.-S., *et al.* (2015). microRNA-33 regulates ApoE lipidation and amyloid-β metabolism in the brain. *J. Neurosci.* **35**, 14717–14726.

Kitazawa, M., Hsu, H.-W., and Medeiros, R. (2016). Copper exposure perturbs brain inflammatory responses and impairs clearance of amyloid-beta. *Toxicol. Sci.* **152**, 194–204.

Lee, S. T., Chu, K., Jung, K.-H., Kim, J. H., Huh, J.-Y., Yoon, H., Park, D.-K., Lim, J.-Y., Kim, J.-M., Jeon, D., *et al.* (2012). miR-206

regulates brain-derived neurotrophic factor in Alzheimer disease model. *Ann. Neurol.* **72**, 269–277.

Lewis, B. P., Burge, C. B., and Bartel, D. P. (2005). Conserved seed pairing, often flanked by adenosines, indicates that thousands of human genes are microRNA targets. *Cell* **120**, 15–20.

Li, Y. Y., Cui, J. G., Hill, J. M., Bhattacharjee, S., Zhao, Y., and Lukiw, W. J. (2011). Increased expression of miRNA-146a in Alzheimer's disease transgenic mouse models. *Neurosci. Lett.* **487**, 94–98.

Liu, C.-C., Hu, J., Zhao, N., Wang, J., Wang, N., Cirrito, J. R., Kanekiyo, T., Holtzman, D. M., and Bu, G. (2017). Astrocytic LRP1 mediates brain Aβ clearance and impacts amyloid deposition. *J. Neurosci.* **37**, 4023–4031.

Liu, C.-G., Wang, J.-L., Li, L., Xue, L.-X., Zhang, Y.-Q., and Wang, P.-C. (2014). MicroRNA-135a and -200b, potential Biomarkers for Alzheimer's disease, regulate β secretase and amyloid precursor protein. *Brain Res.* **1583**, 55–64.

Lucey, B. P., Mawuenyega, K. G., Patterson, B. W., Elbert, D. L., Ovod, V., Kasten, T., Morris, J. C., and Bateman, R. J. (2017). Associations between β-amyloid kinetics and the β-amyloid diurnal pattern in the central nervous system. *JAMA Neurol.* **74**, 207–215.

Lukiw, W. J., Andreeva, T. V., Grigorenko, A. P., and Rogaev, E. I. (2012). Studying micro RNA function and dysfunction in Alzheimer's disease. *Front. Genet.* **3**, 327.

Marques, T. M., Kuiperij, H. B., Bruinsma, I. B., van Rumund, A., Aerts, M. B., Esselink, R. A. J., Bloem, B. R., and Verbeek, M. M. (2017). MicroRNAs in cerebrospinal fluid as potential biomarkers for Parkinson's disease and multiple system atrophy. *Mol. Neurobiol.* **54**, 7736–7745.

Mawuenyega, K. G., Sigurdson, W., Ovod, V., Munsell, L., Kasten, T., Morris, J. C., Yarasheski, K. E., and Bateman, R. J. (2010). Decreased clearance of CNS β-amyloid in Alzheimer's disease. *Science* **330**, 1774.

Medeiros, D. M. (2011). Gastric bypass and copper deficiency: A possible overlooked consequence. *Obes. Surg.* **21**, 1482–1483.

Miller, L. M., Wang, Q., Telivala, T. P., Smith, R. J., Lanzirotti, A., and Miklossy, J. (2006). Synchrotron-based infrared and x-ray imaging shows focalized accumulation of Cu and Zn colocalized with beta-amyloid deposits in Alzheimer's disease. *J. Struct. Biol.* **155**, 30–37.

Morris, M. C., Evans, D. A., Tangney, C. C., Bienias, J. L., Schneider, J. A., Wilson, R. S., and Scherr, P. A. (2006). Dietary copper and high saturated and trans fat intakes associated with cognitive decline. *Arch. Neurol.* **63**, 1085–1088.

Nagaraj, S., Laskowska-Kaszub, K., Dębski, K. J., Wojsiat, J., Dąbrowski, M., Gabryelewicz, T., Kuźnicki, J., and Wojda, U. (2017). Profile of 6 microRNA in blood plasma distinguish early stage Alzheimer's disease patients from non-demented subjects. *Oncotarget* **8**, 16122–16143.

Patterson, B. W., Elbert, D. L., Mawuenyega, K. G., Kasten, T., Ovod, V., Ma, S., Xiong, C., Chott, R., Yarasheski, K., Sigurdson, W., *et al.* (2015). Age and amyloid effects on human central nervous system amyloid-beta kinetics. *Ann. Neurol.* **78**, 439–453.

Prohaska, J. R. (2008). Role of copper transporters in copper homeostasis. *Am. J. Clin. Nutr.* **88**, 826S–829S.

Rembach, A., Hare, D. J., Lind, M., Fowler, C. J., Cherny, R. A., Mclean, C., Bush, A. I., Masters, C. L., and Roberts, B. R. (2013). Decreased copper in Alzheimer's disease brain is predominantly in the soluble extractable fraction. *Int. J. Alzheimers Dis.* **2013**, 623241.

Rodriguez-Ortiz, C. J., Baglietto-Vargas, D., Martinez-Coria, H., LaFerla, F. M., and Kitazawa, M. (2014). Upregulation of miR-181 decreases c-Fos and SIRT-1 in the hippocampus of 3xTg-AD mice. *J. Alzheimers Dis.* **42**, 1229–1238.

Sagare, A. P., Bell, R. D., Zhao, Z., Ma, Q., Winkler, E. A., Ramanathan, A., and Zlokovic, B. V. (2013). Pericyte loss influences Alzheimer-like neurodegeneration in mice. *Nat. Commun.* **4**, 2932.

Salustri, C., Barbati, G., Ghidoni, R., Quintiliani, L., Ciappina, S., Binetti, G., and Squitti, R. (2010). Is cognitive function linked to serum free copper levels? A cohort study in a normal population. *Clin. Neurophysiol.* **121**, 502–507.

Shinohara, M., Tachibana, M., Kanekiyo, T., and Bu, G. (2017). Role of LRP1 in the pathogenesis of Alzheimer's disease: Evidence from clinical and preclinical studies. *J. Lipid Res.* **58**, 1267–1281.

Silbert, L. C., Lahna, D., Promjunyakul, N. O., Boespflug, E., Ohya, Y., Higashiuesato, Y., Nishihira, J., Katsumata, Y., Tokashiki, T., and Dodge, H. H. (2018). Risk factors associated with cortical thickness and white matter hyperintensities in dementia free Okinawan elderly. *J. Alzheimers Dis.* **63**, 365–372.

Silverberg, G. D., Messier, A. A., Miller, M. C., Machan, J. T., Majmudar, S. S., Stopa, E. G., Donahue, J. E., and Johanson, C. E. (2010). Amyloid efflux transporter expression at the blood-brain barrier declines in normal aging. *J. Neuropathol. Exp. Neurol.* **69**, 1034–1043.

Singh, I., Sagare, A. P., Coma, M., Perlmutter, D., Gelein, R., Bell, R. D., Deane, R. J., Zhong, E., Parisi, M., Ciszewski, J., *et al.* (2013). Low levels of copper disrupt brain amyloid-β homeostasis by altering its production and clearance. *Proc. Natl. Acad. Sci. U.S.A.* **110**, 14771–14776.

Son, D. J., Jung, Y. Y., Seo, Y. S., Park, H., Lee, D. H., Kim, S., Roh, Y.-S., Han, S. B., Yoon, D. Y., and Hong, J. T. (2017). Interleukin-32α inhibits endothelial inflammation, vascular smooth muscle cell activation, and atherosclerosis by upregulating Timp3 and Reck through suppressing microRNA-205 Biogenesis. *Theranostics* **7**, 2186–2203.

Song, H., and Bu, G. (2009). MicroRNA-205 inhibits tumor cell migration through down-regulating the expression of the LDL receptor-related protein 1. *Biochem. Biophys. Res. Commun.* **388**, 400–405.

Squitti, R., Barbati, G., Rossi, L., Ventriglia, M., Dal Forno, G., Cesaretti, S., Moffa, F., Caridi, I., Cassetta, E., Pasqualetti, P., *et al.* (2006). Excess of nonceruloplasmin serum copper in AD correlates with MMSE, CSF β-amyloid, and h-tau. *Neurology* **67**, 76–82.

Squitti, R., Ghidoni, R., Siotto, M., Ventriglia, M., Benussi, L., Paterlini, A., Magri, M., Binetti, G., Cassetta, E., Caprara, D., *et al.* (2014). Value of serum nonceruloplasmin copper for prediction of mild cognitive impairment conversion to Alzheimer disease. *Ann. Neurol.* **75**, 574–580.

Squitti, R., Ghidoni, R., Scrascia, F., Benussi, L., Panetta, V., Pasqualetti, P., Moffa, F., Bernardini, S., Ventriglia, M., Binetti, G., *et al.* (2011). Free copper distinguishes mild cognitive impairment subjects from healthy elderly individuals. *J. Alzheimers Dis.* **23**, 239–248.

Storck, S. E., Meister, S., Nahrath, J., Meißner, J. N., Schubert, N., Di Spiezio, A., Baches, S., Vandenbroucke, R. E., Bouter, Y., Prikulis, I., *et al.* (2015). Endothelial LRP1 transports amyloid-β1–42 across the blood-brain barrier. *J. Clin. Invest.* **126**, 123–136.

Sultana, R., Perluigi, M., Newman, S. F., Pierce, W. M., Cini, C., Coccia, R., and Butterfield, D. A. (2010). Redox proteomic analysis of carbonylated brain proteins in mild cognitive impairment and early Alzheimer's disease. *Antioxid. Redox. Signal.* **12**, 327–336.

Talwar, P., Grover, S., Sinha, J., Chandna, P., Agarwal, R., Kushwaha, S., and Kukreti, R. (2017). Multifactorial analysis of a biomarker pool for Alzheimer disease Risk in a North Indian population. *Dement. Geriatr. Cogn. Disord.* **44**, 25–34.

Ventriglia, M., Bucossi, S., Panetta, V., and Squitti, R. (2012). Copper in Alzheimer's disease: A meta-analysis of serum, plasma, and cerebrospinal fluid studies. *J. Alzheimers Dis.* **30**, 981–984.

Vilardo, E., Barbato, C., Ciotti, M., Cogoni, C., and Ruberti, F. (2010). MicroRNA-101 regulates amyloid precursor protein expression in hippocampal neurons. *J. Biol. Chem.* **285**, 18344–18351.

Vogel-Ciernia, A., and Wood, M. A. (2014). Examining object location and object recognition memory in mice. *Curr. Protoc. Neurosci.* **69**, 8.31.1–8.31.17.

Vural, H., Demirin, H., Kara, Y., Eren, I., and Delibas, N. (2010). Alterations of plasma magnesium, copper, zinc, iron and selenium concentrations and some related erythrocyte antioxidant enzyme activities in patients with Alzheimer's disease. *J. Trace Elem. Med. Biol.* **24**, 169–173.

Wu, H. Z., Ong, K., Seeher, K., Armstrong, N. J., Thalamuthu, A., Brodaty, H., Sachdev, P., and Mather, K. (2016). Circulating microRNAs as biomarkers of Alzheimers disease: A systematic review. *J. Alzheimers Dis.* **49**, 755–766.

Wu, Q., Ye, X., Xiong, Y., Zhu, H., Miao, J., Zhang, W., and Wan, J. (2016). The protective role of microRNA-200c in Alzheimer's disease pathologies is induced by beta amyloid-triggered endoplasmic reticulum stress. *Front. Mol. Neurosci.* **9**, 140–140.

Yu, H., Jiang, X., Lin, X., Zhang, Z., Wu, D., Zhou, L., Liu, J., and Yang, X. (2018). Hippocampal subcellular organelle proteomic alteration of copper-treated mice. *Toxicol. Sci.* **164**, 250–263.

Yue, X., Lan, F., Hu, M., Pan, Q., Wang, Q., and Wang, J. (2016). Downregulation of serum microRNA-205 as a potential diagnostic and prognostic biomarker for human glioma. *J. Neurosurg.* **124**, 122–128.

Zhao, Y., Bhattacharjee, S., Jones, B. M., Hill, J., Dua, P., and Lukiw, W. J. (2014). Regulation of neurotropic signaling by the inducible, NF-kB-sensitive miRNA-125b in Alzheimer's disease (AD) and in primary human neuronal-glial (HNG) cells. *Mol. Neurobiol.* **50**, 97–106.

Zhao, Z., Sagare, A. P., Ma, Q., Halliday, M. R., Kong, P., Kisler, K., Winkler, E. A., Ramanathan, A., Kanekiyo, T., Bu, G., *et al.* (2015). Central role for PICALM in amyloid-β blood-brain barrier transcytosis and clearance. *Nat. Neurosci.* **18**, 978.